Version 10/12/99 - Submitted to AJ

A Blind H I Survey for Galaxies in the Zone of Avoidance, $308° \leq \ell \leq 332°$.

S. Juraszek,[1,2] L. Staveley-Smith,[2] R.C. Kraan-Korteweg,[4] A.J. Green,[1] R.D. Ekers,[2] R.F. Haynes,[2] P.A. Henning,[3] M.J. Kesteven,[2] B. Koribalski,[2] R.M. Price,[3] E.M. Sadler,[1] A. Schröder[5]

ABSTRACT

We report on a blind neutral hydrogen survey for galaxies using the 21 cm multibeam receiver on the Parkes 64 m telescope. The surveyed region covers $|b| \leq 5°$ in the Zone of Avoidance (ZOA) from Galactic longitude 308° to 332°. The survey represents the first phase of a blind H I survey covering the southern ZOA ($l = 212°$ to 36°). We have detected H I in 42 galaxies above a 3σ limit of 60 mJy. The galaxies detected in this survey have velocities out to 6000 km s^{-1} and H I masses in the range 4×10^7 to 3×10^{10} M$_\odot$ (h_{75}^{-2}). Only 8 of the 42 galaxies have velocities previously measured. A further 9 galaxies appear to have optical counterparts in the catalog of Woudt (1998). In total, 16 of the galaxies appear to be associated with IRAS sources, although only 3 of these are without optical counterparts. The estimated median extinction for the 20 galaxies with optical or IR counterparts is $A_B = 3.8$ mag. For the 22 galaxies with no counterparts, the estimated median extinction is $A_B = 5.6$ mag. The distribution of galaxies is suggestive of a connection between the Centaurus supercluster above the Galactic Plane and the Pavo-Indus supercluster beneath the Plane. No previously hidden concentrations of galaxies were found.

Subject headings: surveys – galaxies: distances and redshifts – galaxies: fundamental parameters – radio lines: galaxies

1. Introduction

Historically, astronomers have not studied large-scale structures close to the Galactic Plane due to the obscuring effects of dust and high stellar density. The size of this Zone of Avoidance

[1]School of Physics, University of Sydney, NSW 2006, Australia

[2]Australia Telescope National Facility, CSIRO, P.O. Box 76, Epping, NSW 2121, Australia

[3]Institute for Astrophysics, University of New Mexico, 800 Yale Blvd, NE, Albuquerque, NM 87131, USA

[4]Departemento de Astronomia, Universidad de Guanajuato, Apartado Postal 144, Guanajuato, Gto 36000, Mexico

[5]Observatoire de la Côte d'Azur, B.P.4229, 06304 Nice Cedex 4, France

(ZOA) varies with Galactic longitude and observing wavelength. One estimate of its extent (Lahav 1994) suggests that ~20% of the sky in the optical and ~10% in the infrared are obscured. As a result of this obscuration, very little systematic and uniform data on galaxy distributions exist for $|b| < 10°$. A complete picture of the galaxy distribution is essential for studies of nearby large-scale structure and its effect on the motion of the Local Group of galaxies. For example, Kolatt, Dekel & Lahav (1995) find that the mass distribution for ZOA galaxies out to 6000 km s^{-1} strongly affects the direction of the predicted gravitational acceleration at the position of the Local Group. Marinoni et al. (1998) also point out that their predicted barycenter for the massive Shapley supercluster, based on the Mark III peculiar velocity catalog (Willick et al. 1997), is only 4° from the Galactic equator, and is well separated from the canonical optical center.

Over the past decade, in particular, many attempts have been made to penetrate the ZOA and detect galaxies. Optical plates have been searched effectively in this area (Kraan-Korteweg & Woudt 1994; Saitō et al. 1990, 1991 and Wakamatsu et al. 1994), down to $|b| \sim 4°$. A combination of optical and near-IR imaging appears to extend the possibility of galaxy detection to around $|b| \sim 3°$. Far-infrared (FIR) color selection of sources in the IRAS Point Source Catalog (Version 2, 1998, hereafter PSC) has been moderately successful in selecting candidate galaxies at lower Galactic latitudes, $|b| > 2°$ (Lu et al. 1990, Saunders et al. 1994). Though these methods still rely on follow-up observations of candidates for confirmation (e.g. in H I, Bottinelli et al. 1994), as IRAS observations become confusion-limited close to the Plane. For $|b| < 5°$ all optical and infrared observations become very difficult to determine and are ultimately confusion-limited. However, in this latitude range, λ21 cm observations have been very successful in finding galaxies.

Blind H I Surveys for galaxies hidden by the Milky Way were pioneered by Kerr & Henning (1987) on the Green Bank 300 foot telescope, and have continued on the Dwingeloo 25 m telescope (Henning et al. 1998). However, such H I surveys have been severely limited in either sensitivity or area of sky that can be surveyed. The development of a 21 cm multibeam receiver for the Parkes 64 m telescope[6] has changed matters. This receiver has an array of 13 feed horns (each having two receivers observing orthogonal linear polarisations) mounted in a hexagonal pattern in the prime focus (Staveley-Smith et al. 1996) and allows large areas to be surveyed at adequate sensitivity in a relatively short time.

The region of sky investigated here was chosen for several reasons. The large-scale structures that we see above the Galactic Plane (Centaurus at $\ell \approx 302°$, $b \approx 22°$) and below the Plane (Pavo at $\ell \approx 332°$, $b \approx -24°$) have long suggested that a connection may exist behind our Galactic Plane (Lahav 1994). The galaxy counts along this structure continue to increase towards the ZOA suggesting higher densities of galaxies may be expected. A massive galaxy cluster (Abell 3627) has been rediscovered (Kraan-Korteweg et al. 1996) to lie along this structure at $b = -7°$. This entire region has already been searched by visual inspection for galaxies by Woudt (1998), who was

[6]The Australia Telescope is funded by the Commonwealth of Australia for operation as a National Facility managed by CSIRO.

successful in identifying galaxies at latitudes of $|b| > 4°$. It is also of interest as it may shed light on existence or nature of the Great Attractor, predicted by Kolatt et al. (1995) and Lynden-Bell et al. (1988) to lie near the centre of this field.

In § 2, the H I observations and data reduction are discussed. In § 3 we discuss the galaxy detection method and list the detected objects together with their properties. We examine the optical and IR cross-identifications in § 4. Finally in § 5 we discuss the global properties of the galaxies, examine their 3-dimensional distribution and their relationship with previously known large-scale structures.

2. Observations and Data Reduction

The systematic blind H I survey of the southern ZOA began using the Parkes 64 m telescope in 1997 March 22, and is expected to be completed late in 2000 (Staveley-Smith et al. 1998). The relevant observations presented here were made during March to May 1997. These data represent about 16% of the final survey integration time and 17% of the area coverage. The ZOA "shallow survey" of Henning et al. (1999) covers the entire southern ZOA, but with only 8% of the final survey integration time. The 21 cm multibeam instrument has a beamwidth of 14$'\!.$3 (FWHP) and the receiver system temperature is 20 K on average. The multibeam correlator has a bandwidth of 64 MHz and covers the frequency range of 1362.5 to 1426.5 MHz. This corresponds to a velocity (cz) range of -1200 to 12700 km s^{-1}. The channel spacing is 13 km s^{-1}. The sensitivity in the velocity range between -100 to +100 km s^{-1} is significantly lower due to Galactic H I. The velocity resolution is 18 km s^{-1} or 26 km s^{-1} for Hanning-smoothed data (discussed in § 3.2).

Three standard fields, $8° \times 10°$ in size and centered on Galactic longitudes 312°, 320° and 328° make up the data for the 240 square degree field presented here. The observations are Nyquist sampled and then gridded together into a single cube using specially developed AIPS++ routines (Barnes 1998).

Each of the 3 standard data fields, which make up the data cube, has been observed on four occasions following the scan pattern shown in Figure 1. Each field is made up of 17 scans with each scan being equivalent to an observation of one strip in Galactic longitude, 1$^\circ\!.$7 wide and 8° long. The receiver is rotated 15° with respect to the Galactic equator and each subscan is translated $35'$ in Galactic latitude. This results in full Nyquist-sampling of the sky and an effective integration time for each point, over the whole region $308° \leq l \leq 332°$, $-5° \leq b \leq +5°$ of 200 s. The final data cube has an rms noise of 20 mJy beam^{-1} (without Hanning smoothing).

The data were bandpass-calibrated, velocity-shifted to the heliocentric frame and baseline-subtracted (DC offset only) using a realtime system based on AIPS++ (Barnes et al. 1998). Then a 'top-hat' median gridding algorithm with top-hat radius of $6'$ was used. The post-gridding beamwidth is 15$'\!.$5 and the pixel size in the cubes is $4' \times 4'$. Further data inspection and analysis were carried out MIRIAD[7] and the KARMA visualisation tool KVIEW (Gooch 1995).

3. Cube Analysis and Results

3.1. Search method

The data cube was searched visually. No Hanning smoothing was applied and only zero'th order baseline subtraction was used. KVIEW was used to inspect the data cube, which was searched in all the three possible planes i.e. along the RA, Dec and velocity axis respectively. Sources which were found in only one of the above planes were rechecked and often not confirmed – noise and interference are the principal reason for false detections.

The application of this process resulted in a catalog of candidate sources for H I galaxies. We then used the MIRIAD task IMSTAT to determine the cube rms noise in patches free of detectable sources. The lower peak brightness limit for the final catalog was then set at 3 times the rms noise per channel (60 mJy beam^{-1}) for the unsmoothed data.

3.2. Galaxy Properties

In Table 1 all the relevant H I data and derived properties of the 42 galaxies found in the blind survey have been compiled. The Hanning smoothed H I profiles of the detected galaxies are illustrated in Figure 2.

An explanation of the parameters displayed in Table 1 follows.

Column 1: Source name. Sources marked by (^{a}) have more accurate ATCA data listed in Staveley-Smith et al. (1998).

Columns 2 & 3: Equatorial coordinates (J2000). This is the Gaussian-fitted position of the H I source, using a total intensity image. The resulting positional uncertainty of the source is $\sim 3'$.

Columns 4 & 5: Galactic coordinates corresponding to the source position.

Column 6: The velocity (cz) is in the heliocentric reference frame. The radial velocity (km s^{-1}) corresponds to the midpoint of the H I profile calculated at 50% of the peak brightness value. The uncertainty in the velocity is 10 km s^{-1}.

Column 7: Velocity width at 50% peak brightness. The velocity width for each source was calculated from the spectra obtained from IMSPEC. A constant correction of 6 km s^{-1} was subtracted from the velocity widths to compensate for instrumental resolution of 18 km s^{-1} and

[7] Multichannel Image Reconstruction, Image Analysis and Display package (Sault, Teuben & Wright 1995).

based on a dispersion of the H I gas of about 10 km s^{-1}. Similar corrections are applied by Fisher & Tully (1981). The uncertainty for 50% widths is 20km s^{-1}.

Column 8: Distance (d), with respect to the Local Group

$H_{\circ}$ d $= cz + 300 \sin l \cos b$

We assume a $H_{\circ} = 75$ km s^{-1} Mpc^{-1} throughout this paper. No corrections were made for streaming motions.

Column 9: Integrated flux densities (in units of Jy km s^{-1}) were calculated using MIRIAD. A total power image was created for each source by combining (adding) velocity planes. The range in velocity used was detemined by the velocity width of the source defined in Column 5 above. The source flux was then spatially integrated. The rms uncertainty in the integral is typically 20%, but larger in the case of objects with weak profiles and residual baseline curvature as shown in Figure 2.

Column 10: H I mass of source, calculated from the integrated flux density and distance.

Figure 2 shows the H I velocity profiles of each source from Table 1. The velocity axis is in km s^{-1} (cz). The spectrum for each source was calculated by MIRIAD task IMSPEC over a given region of the source. The spectra have been Hanning smoothed.

Of the 42 galaxies above, four galaxies are well resolved by the Parkes beam. If the effective major axis of the galaxy was measured to be larger than $22'$, then the source is listed as resolved and a H I diameter is measured. This allowed a calculation of the total mass of the galaxy (Table 2), which is a lower limit in the case of the three galaxies without measured inclinations. Table 2 lists the properties of the four galaxies. The columns are:

Column 1: Source name, as in Table 1.

Column 2: The H I diameter of the source measured at the 50% peak column density contour level.

Column 3: The lower limit to the total mass

$M_T = 2.33{\times}10^5\ R_{kpc}\ V_{rot}^2$

as used here, assumes a rotational velocity (V_{rot}) that is approximated by $V_{rot} = 0.5\ \Delta V_{50}\ (\csc i)$

The inclination (i) has been obtained from the WKK (Woudt 1998) catalog (described in § 4.1). If an optical counterpart could not be found an inclination of 90° is assumed (^{a}) and the mass is a lower limit.

Column 4: H I mass to total mass ratio, expressed as a percentage.

Column 5: Estimate of morphology, based on the H I mass-to-total mass ratio in column

4 and the values listed in Roberts & Haynes (1994). The morphology classification of HIZOA J1616-55 is extremely uncertain.

3.3. Unusual Systems

Several of the detected galaxies have very unusual characteristics, suggesting interactions or mergers in progress, three of which are:

HIZOA J1416-58: this is a low H I flux (peak brightness $\sim$ 70 mJy) galaxy with a huge velocity width of 685 km s^{-1}. Follow-up observations are underway with the ATCA.

HIZOA J1532-56 is the first galaxy found to have a Galactic latitude of 0.0° in the area of the Great Attractor. It is hidden by 70 mag of extinction in B-band as given by the 100μm DIRBE/IRAS maps (Schlegel, Finkbeiner & Davis 1998). It appears well-resolved by the Parkes beam and shows unusual structure in the velocity planes. This galaxy has already been observed with ATCA (Staveley-Smith et al. 1998), showing it to be an interacting system.

HIZOA J1616-55: this system is nearby (3.3 Mpc, v=403 km s^{-1}) and large (44 kpc). Although classified as an LSB type (Table 2), observations with the ATCA (Staveley-Smith et al. 1998) have shown that it is likely to be an interacting pair of low mass H I galaxies.

4. Optical and Far-Infrared Cross Identifications

4.1. Optical Counterparts

In looking for optical counterparts to the H I detected galaxies we define:
(a) *associations* - optically identified sources which are within a 6′ radius of the H I position;
(b) *identifications* - sources which are within a 6′ radius of the H I position and which have measured velocities in agreement with the H I velocities. This terminology is used throughout this paper.

The search for optical counterparts was made in two ways: first using NED[8], then using the WKK optical catalogue. The WKK galaxies were identified by visual inspection of IIIaJ film copies of the SRC sky survey (Woudt 1998). This search resulted in identifying 8 galaxies and a further 9 associations.

Table 3 lists the known optical parameters of the candidates. The columns are:

Column 1: Source name, as in Table 1.

[8]The NASA/IPAC Extragalactic Database (NED) is operated by the Jet Propulsion Laboratory, California Institute of Technology, under contract with the National Aeronautics and Space Administration.

Column 2: Optical association Name. All ESO galaxies shown have also been correlated with WKK galaxies.

Column 3: Radial offset in arcmin from H I position.

Column 4: Velocity (cz) in km s^{-1}. Velocities shown for WKK galaxies are from Woudt & Kraan-Korteweg (2000) and those for ESO galaxies are from NED. Velocities marked with (^{a}) are not yet published and may not be final.

Column 5: Inclination angle calculated according to Holmberg (1946):

$\cos^2 i = (r^2 - r_\circ^2)(1 - r_\circ^2)^{-1}$

where r is the observed minor/major axial ratio ($\frac{b}{a}$) and $r_\circ$ is the intrinsic flattening. We assume $r_\circ = 0.2$ (e.g. Richter & Huchtmeier (1984). The inclinations are most likely lower limits compared to the true inclinations (Kraan-Korteweg 1992) as extinction obscures the extent of the faint disks more effectively then the bulges.

Column 6: Estimate of morphological type as given by the WKK or ESO catalogues. The ESO galaxy classification has been confirmed with the WKK catalogue morphology classifications.

Column 7: B_J magnitude as given in Woudt (1998).

Column 8: B-Band extinction in magnitudes derived from the 100μm DIRBE/IRAS data (Schlegel et al. 1998) for each H I position. These data provide a direct measure of the dust column density. Therefore, in this case, the gas-to-dust ratio is not important. We have used the DIRBE/IRAS data to determine extinction instead of H I column densities because the Galactic H I line might be saturated and therefore give an underestimate of the value for extinction at these latitudes. We do note that the DIRBE/IRAS data are not well calibrated in the ZOA and should be used with caution.

4.2. IRAS Counterparts

As most of the galaxies we have detected are totally obscured optically, we look for infrared associations to gain a better understanding of the galaxies. We have done this in three ways:
(i) IRAS PSC associations with optically identified galaxies;
(ii) IRAS PSC associations with H I galaxy positions; and
(iii) examining the IRAS Galaxy Atlas (IGA, Cao et al. 1997) data.

We first searched the Woudt (Woudt 1998) catalog of optically identified galaxies. This catalog has already been cross correlated with the IRAS PSC using a search radius of $2'$. The search resulted in 13 H I galaxies having both optical and infrared associations, 3 having tentative IRAS associations and 4 having only optical associations.

Those galaxies for which we did not find any association in the Woudt catalogue were looked at in the IRAS PSC with a $6'$ search radius. The search resulted in a list of possible IRAS associations. In some cases more then one infrared source was found in the search radius. To determine if the IRAS source could be a real association we have used two further selection criteria: (*i*) the source must have 2 or more flux densities out of the 4 IRAS bands (i.e. we do not accept sources with only one flux density and three upper limits); and (*ii*) it must have IRAS color characteristics of a galaxy (Yamada et al. 1993a,b). Sources that fail these criteria have been dropped from Table 4.

Finally we have used the IGA (super-resolved IRAS data). The IGA has a resolution of $1' - 2'$, and provides a three-fold improvement in linear resolution relative to the IRAS Sky Survey Atlas (ISSA). This was of particular interest as in some cases there were several faint sources in the region of the H I contours. We overlayed H I total intensity contours over the IGA at both 60 and 100μm bands. This allowed us to determine whether any of the IRAS associations that were rejected by criterion (*i*) were real. Four such IRAS sources were found in the IGA images. For these source fluxes were calculated from the IGA data. Also upper limits at 100μm for 3 IRAS sources, which passed our criteria, have been revised and recalculated from the IGA.

The integrated flux densities from the IGA bands (IGA fluxes were first converted to Jy pixel^{-1}) were calculated using MIRIAD task CGCURS by integrating over a patch of the visible extent of the source. To subtract any background due to the Galaxy, an annulus was made around the source, avoiding any other source flux. This was used to calculate average and maximum flux for the background.

Table 4 lists the IRAS associations made with the H I galaxies and their flux densities.

Column 1: Source name, as in Table 1.

Column 2: The IRAS association name from the IRAS PSC.

Column 3: Radial offset of the IRAS source from the H I position.

Columns 4,5,6,7: IRAS flux densities in the 12, 25, 60, 100μm IRAS bands, and their uncertainties. 16 galaxies have been associated with IRAS PSC sources fulfilling the requirements described in this section.

4.3. H I positional accuracy

The difference between the H I and optical/IRAS position, in Right Ascenstion (R.A.) and Declination (Dec.) coordinates, is shown in Figure 3. The mean R.A. offset is $1\overset{'}{.}7$ with an rms of $1\overset{'}{.}4$, and in Dec. it is $1\overset{'}{.}6$ and $1\overset{'}{.}1$ respectively. This corresponds to between 10 and 20% of the $14\overset{'}{.}3$ FWHP beam of the Parkes telescope. There may be a small number of false associations. This will be further investigated in the full sensitivity survey data.

5. Discussion

The 42 detected galaxies have an H I mass range between about 4×10^7 and 3×10^{10} M$_\odot$ (h_{75}^{-2}). Assuming a mean linewidth of 100 km s^{-1}, the H I mass limit at the 3σ level is $M_{HI} = 1.5 \times 10^6\ d^2_{Mpc}$ M$_\odot$. Figure 4 shows the approximate lower H I mass limit for each velocity in our range.

Although only 8 have been previously cataloged with velocities, we have tentatively found optical and far-infrared counterparts for a further 12 galaxies. The median extinction for the 20 galaxies with counterparts is $A_B = 3.8$ mag (Table 3). For the remaining unidentified galaxies, it is $A_B = 5.6$ mag. The fact that some galaxies with apparently moderate extinction (< 4 mag) are unidentified is perhaps not surprising, owing to the preference for H I-selected samples to favour low optical surface brightness objects. However, it should also be noted that the Schlegel et al. (1998) extinctions are poorly calibrated in the Plane.

The galaxies range in velocity up to 6000 km s^{-1} as shown in the histogram in Figure 5. This upper limit corresponds to the sensitivity limit of the existing data (the final ZOA survey will have six times more integration time). The histogram shows distinct peaks at 1250, 3000 and 5250 km s^{-1}. Although, due to the limited nature of the sample, the statistical significance of the suggested overdensities in Figure 5 is low, nevertheless the first two redshift peaks seem to match the expected peaks due to the Local Supercluster and the Centaurus and Pavo superclusters, respectively. In our sample, the main concentration of galaxies (45%) is in the velocity range 2500 to 4000 km s^{-1} as might be expected if there exists a continuous bridge of galaxies stretching between the Centaurus and Pavo superclusters behind the Galactic Plane.

The spatial distribution of the galaxies is shown in Galactic coordinates in Figure 6. The galaxies with optical and IRAS associations populate the diagram away from 0° latitude. Galaxies with only a H I detection lie closer to 0°, although they may still be discriminated against owing to higher system temperatures and continuum confusion within a degree of the Plane. The distributions in velocity (Figure 5) and on the sky (Figure 6) become more interesting when plotted with previously published data over a wider region. The distribution of all optically identified galaxies within 6000 km s^{-1}, as given by the Lyon-Meudon Extragalactic Data Base[9] (LEDA), is shown in Figure 7 together with the new galaxies. The Centaurus (302°, 22°) and Pavo II (332°, −24°) clusters are clearly seen, but the A3627 overdensity at (325°, −7°) is not so clearly seen in the LEDA data. However, the new detections show some evidence for continuity of the Centaurus filamentary structure, a continuous bridge of galaxies stretching from the Centaurus supercluster, behind the ZOA, in the general direction of the Pavo cluster.

The galaxies detected along the suggested Centaurus-Pavo bridge are better seen in the cone diagrams shown in Figure 8. From the Centaurus cluster, there seems to be an increase of median

---

[9]We have made use of the Lyon-Meudon Database (LEDA) supplied by the LEDA team at the CRAL-Observatoire de Lyon (France).

redshift as longitude increases and latitude decreases in such a manner that a continuous bridge is again suggested. The new H I data, when considered alone, suggest a more continuous cellular structure from 3000 to 6000 km s^{-1}, with Centaurus at the edge of the cell wall. However, the combined data show a more complex structure which is undoubtedly due, in part, to the patchy and incomplete nature of the optical redshift observations.

Given the caveats about the completeness and shallowness of the present survey, it is of interest to compare the present data with the POTENT prediction by Kolatt et al. (1995) that the central peak of the Great Attractor should lie at $(l, b, cz) = (320°, 0°, 4000$ km s$^{-1})$. Whilst a broad overdensity exists at $\sim$ 4000 km s^{-1} in the current data (Figure 5), there is no compelling evidence for any discrete structure, previously hidden by the Galactic Plane, providing the bulk of the Great Attractor mass. The best candidate for this remains the A3627 cluster (Kraan-Korteweg et al. 1996), though, with an estimated mass of $0.4 - 2.2 \times 10^{15}$ M$_\odot$ (Boehringer et al. 1996), the cluster itself provides only a small part of the gravitational acceleration required to explain the motions of galaxies in the nearby Universe.

6. Summary

We have cataloged positions and redshifts for 42 galaxies in a blind H I survey of a small part of the southern Zone of Avoidance (ZOA). Only 8 of these have previous redshifts, although a subsequent search at the H I positions has led to a further 12 (some tentative) optical or IRAS associations. The H I data allow galaxies to be found closer to the Galactic Plane than previously possible. The H I data show that there exists a general overdensity of galaxies between 2500 and 4000 km s^{-1}, suggestive of a continuous bridge of galaxies stretching between the Centaurus and Pavo superclusters behind the Galactic Plane. However, no dramatic new structure is revealed in the velocity and H I mass range explored here. The full-sensitivity multibeam survey of this, and surrounding ZOA regions is underway and should allow us to extend the redshift range of the search and better quantify the apparent overdensity of galaxies.

We thank members of the HIPASS team for their tremendous observing assistance, Ian Stewart and many others at Parkes for their support at the telescope, and Taisheng Ye, David Barnes, Richard Gooch and the AIPS++ team for software support. We thank Patrick Woudt for the use of the WKK catalogue from his PhD thesis. Sebastian Juraszek would like to acknowledge partial support from an ARC scholarship. The research of Dr P.A. Henning is supported by NSF Faculty Early Career Development (CAREER) Program award AST 95-02268.

REFERENCES

Barnes, D.G. 1998, in ASP Conf. Ser. 145, Astronomical Data Analysis Software and Systems VII, ed. R. Albrecht, R. N. Hook, & H. A. Bushouse (San Francisco: ASP), 32

Barnes, D.G., Staveley-Smith, L., Ye, T., & Oosterloo, T. 1998, in ASP Conf. Ser. 145, Astronomical Data Analysis Software and Systems VII, ed. R. Albrecht, R. N. Hook, & H. A. Bushouse (San Francisco: ASP), 89

Beichman, C.A., Neugebauer G., Habing H.J., Clegg P.E., & Chester T.J. 1985, Explanatory Supplement to the IRAS Catalogues and Atlases, US Government Printing Office, Washington DC

Boehringer, H., Neumann, D.M., Schindler, S., & Kraan-Korteweg, R.C. 1996, ApJ, 467, 168

Bottinelli, L., Gouguenheim, L., Loulergue, M., Martin, J.M., Theurean, G., Paturel, G. 1994, in ASP Conf. Ser. 67, Unveiling Large-Scale Structures behind the Milky Way, ed. C. Balkowski, & R. C. Kraan-Korteweg (San Francisco: ASP), 225

Cao, Y., Terebey, S., Prince, T. A. & Beichman, C. A. 1997, ApJS, 111, 387

Fisher, J.R. & Tully, R.B. 1981, ApJS, 47, 139

Gooch, R.E. 1995, Workshop on Applications of Radio Science, Australia Academy of Science through the National Committee for Radio Science

Henning, P.A., Kraan-Korteweg, R.C., Rivers, A.J., Loan, A.J., Lahav, O., & Burton, W.B. 1998, AJ, 115, 584

Henning, P.A., Staveley-Smith, L., Ekers R., Green, A.J., Haynes, R., Juraszek, S., Kesteven, M., Koribalski, B., Kraan-Korteweg, R.C., Price, M., Sadler E.M., Schroder, A. 1999, AJ, in preparation

Holmberg E. 1946, Medd. Luna Obs. II, 117

IRAS Point Source Catalogue Version 2, Joint IRAS Science Working Group (eds.) 1988, GPO, Washington DC

Kerr, F.J., & Henning, P.A. 1987, ApJ, 320, L99

Kolatt, T., Dekel, A., & Lahav, O. 1995, MNRAS, 275, 797

Kraan-Korteweg, R.C. & Huchtmeier, W.K. 1992, A&A, 266, 150

Kraan-Korteweg, R.C. & Woudt, P.A. 1994, in ASP Conf. Ser. 67, Unveiling Large-Scale Structures behind the Milky Way, ed. C. Balkowski, & R. C. Kraan-Korteweg (San Francisco: ASP), 89

Kraan-Korteweg, R.C., Woudt, P.A., Cayatte, V., Fairall, A.P., Balkowski, C. & Henning P.A. 1996, Nature, 379, 519

Lahav, O. 1994, in ASP Conf. Ser. 67, Unveiling Large-Scale Structures behind the Milky Way, ed. C. Balkowski, & R. C. Kraan-Korteweg (San Francisco: ASP), 7

Lynden-Bell, D., Faber, S.M., Burstein, D., Davies, R. L., Dressler, A., Terlevich, R.J., & Wegner, G. 1988, ApJ, 326, 19

Lu, N.Y., Dow, M.W., Houck, J.R., Salpeter, E.E., & Lewis, B.M. 1990, ApJ, 357, 388

Marinoni, C., Monaco, P., Giuricin, G., & Costantini, B. 1998, ApJ, 505, 484

Richter, O.G., & Huchtmeier, W.K. 1984, A&A, 132, 253

Roberts, M.S., & Haynes, M.P. 1994, ARA&A, 32, 115

Saitō, M., Ohtani, H., Asonuma, A., Kashikawa, N., Maki, T., Nishida, S., & Watanabe, T. 1990, PASJ, 42, 603

Saitō, M., Ohtani, H., Baba, A., Hotta, H., Kameno, S., Kurosu S., Nakada, L., & Takata, T. 1991, PASJ, 43, 449

Sault, R.J., Teuben P.J., & Wright M.C.H. 1995, in ASP Conf. Ser. 77, Astronomical Data Analysis Software and Systems IV, , ed. R.A. Shaw, H.E. Payne, & J.J.E. Hayes (San Francisco: ASP), 433

Saunders, W., Sutherland, W.J., Efstathiou, C., Tadros, H., Maddox, S., Mcmahon, R.G., White, S.D.M., Rowan-Robinson, M., Oliver, S.J., Keeble, O., Frenk, C.S., & Smoker, J.V. 1994, in ASP Conf. Ser. 67, Unveiling Large-Scale Structures behind the Milky Way, ed. C. Balkowski, & R. C. Kraan-Korteweg (San Francisco: ASP), 257

Schlegel, D.J., Finkbeiner, D.P. & Davis, M. 1998, ApJ, 500, 525

Staveley-Smith, L., Wilson, W.E., Bird, T.S., Disney, M.J., Ekers, R.D., Freeman, K.C., Haynes, R.F., Sinclair, M.W., Vaile, R.A., Webster, R.L., & Wright, A.E. 1996, PASA, 13, 243

Staveley-Smith, L., Juraszek, S., Koribalski, B.S., Ekers, R.D., Green, A.J., Haynes, R.F., Henning, P.A., Kesteven, M.J., Kraan-Korteweg, R.C., Price, R.M. & Sadler, E.M. 1998, AJ, 116, 2717

Wakamatsu, K., Hasegawa, T., Karoji, H., Sekiguchi, K., Menzies, J.W., Malkan, M. 1994, in ASP Conf. Ser. 67, Unveiling Large-Scale Structures behind the Milky Way, ed. C. Balkowski, & R. C. Kraan-Korteweg (San Francisco: ASP), 131

Willick, J.A., Courteau S., Faber, S.M., Burstein D., Dekel, A., & Strauss, M.A. 1997, ApJS, 109, 333

Woudt, P.A., & Kraan-Korteweg, R.C. 2000, in preparation

Woudt, P.A. 1998 Ph.D. thesis, Univ. of Cape Town

Yamada, T., Takata, T., Djamaluddin, T., Tomita, A., Aoki, K., Takeda, A., & Saitō, M. 1993a, MNRAS, 262, 79

Yamada, T., Takata, T., Djamaluddin, T., Tomita, A., Aoki, K., Takeda, A., & Saitō, M. 1993b, ApJS, 89, 57

This preprint was prepared with the AAS LATEX macros v4.0.

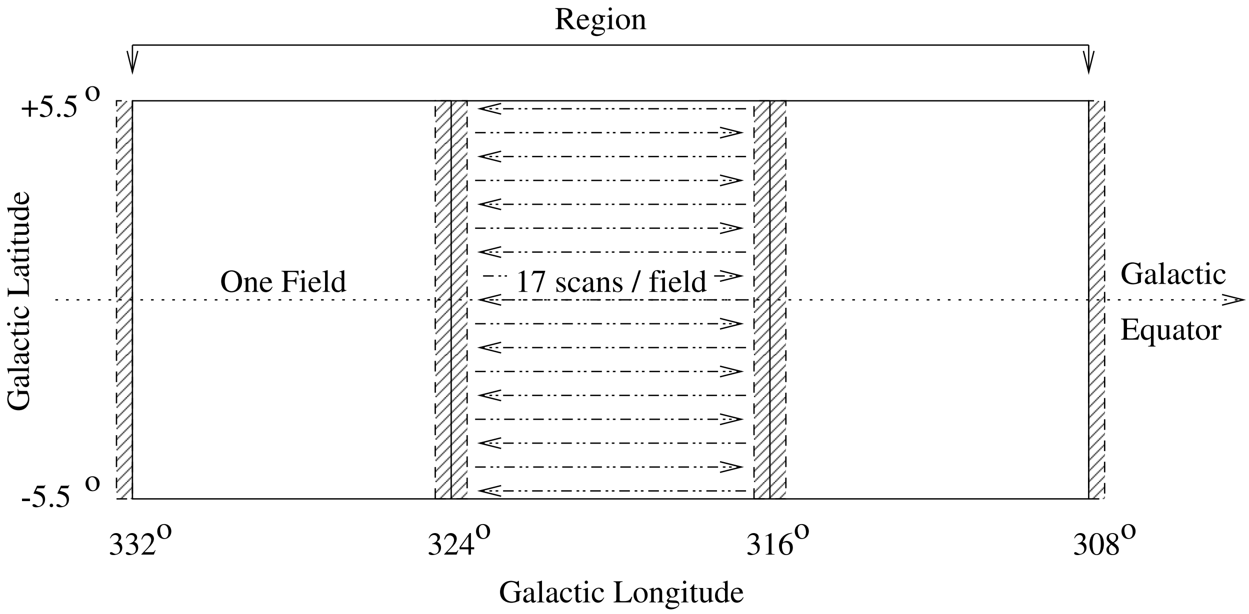

Fig. 1.— The region surveyed. One field (an 8° × 10° area) is scanned in Galactic longitude 17 times. Each field overlaps the next by ∼ 2°. The fields are then mosaiced to form the whole region.

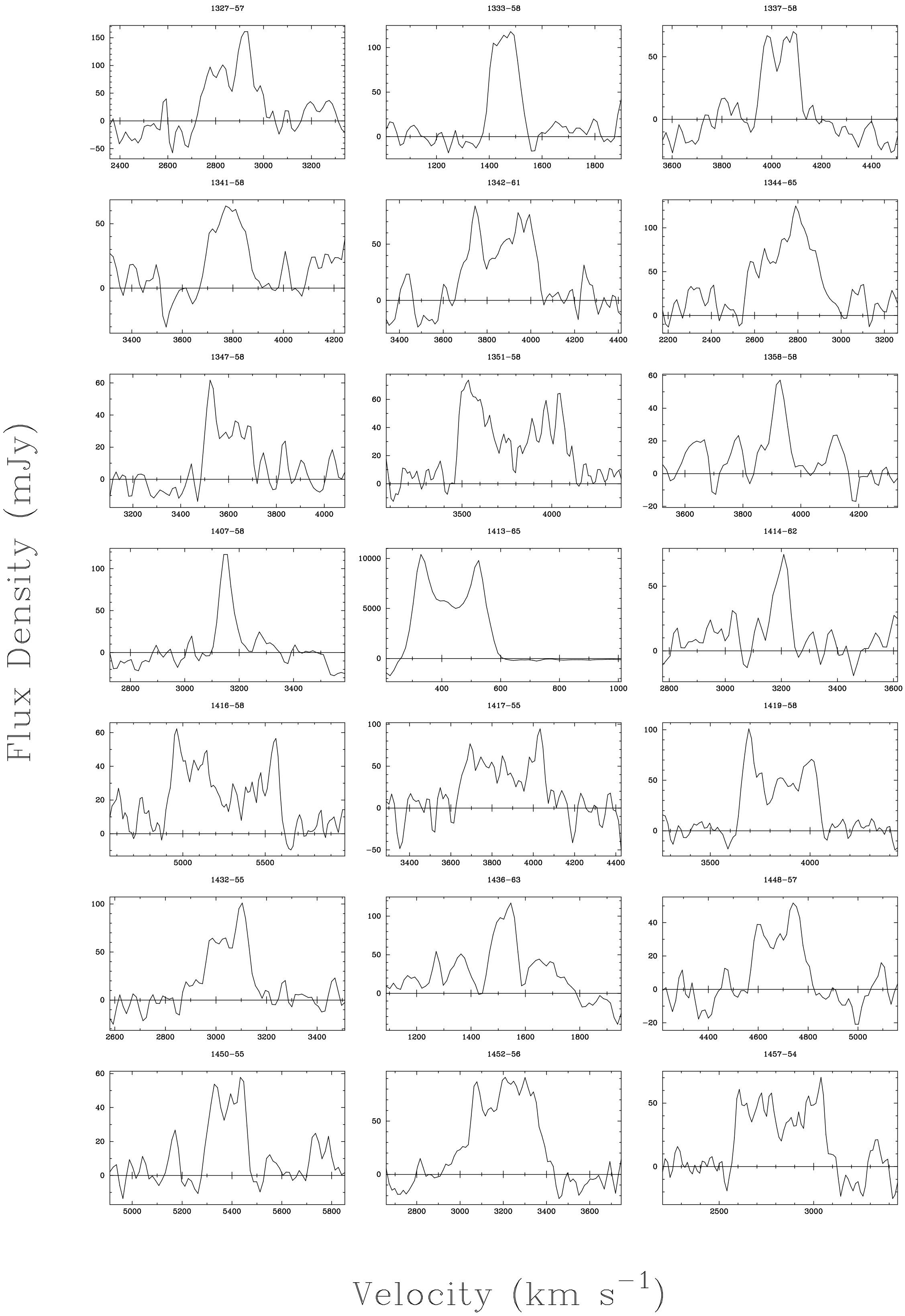

Fig. 2.— Integrated HI line profiles of the 42 galaxies detected in the survey.

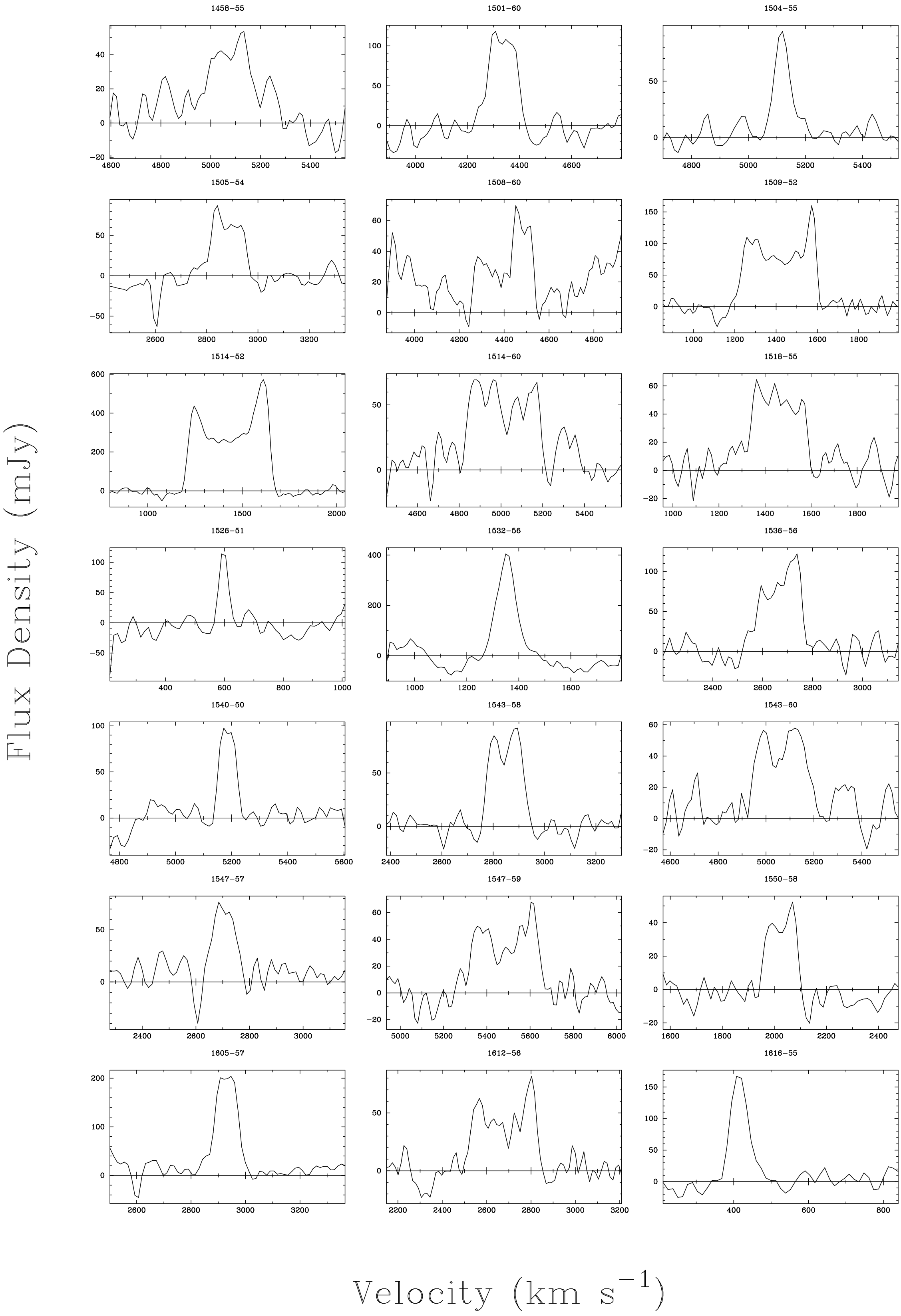

Fig. 2.— Continued.

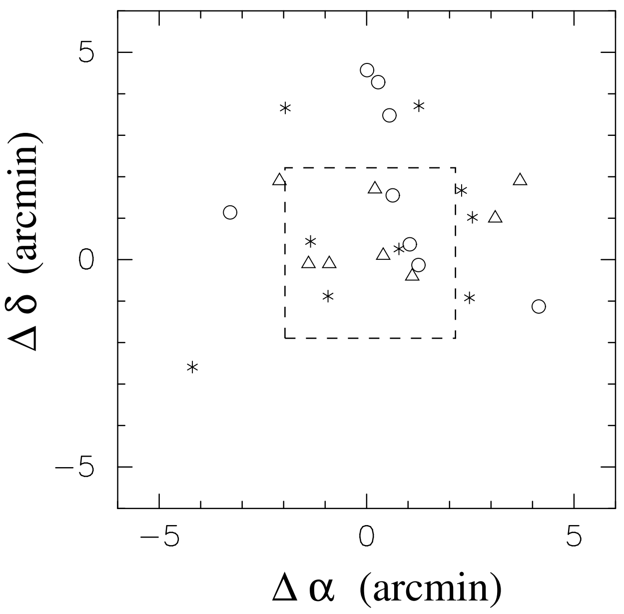

Fig. 3.— The offset between the HI position and optical or IRAS association. The dashed line marks the size of a single $4' \times 4'$ pixel from the HI data. ○ : galaxies which have been optically identified (position and redshift coincidence). △ : galaxies associated with IRAS sources. ∗ : galaxies with optical associations (position coincidence only).

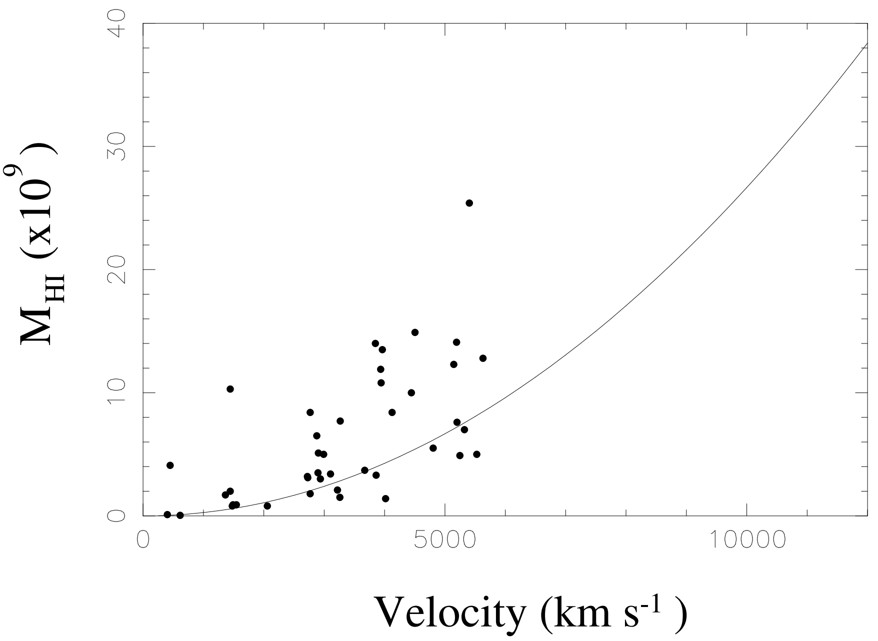

Fig. 4.— The line shows the approximate lower limit to the H I mass as a function of velocity assuming a flux density of 60 mJy and linewidth of 100 km s^{-1}. Dots mark the H I detected galaxies. Some fall below the line as their velocity widths are less the 100 km s^{-1}.

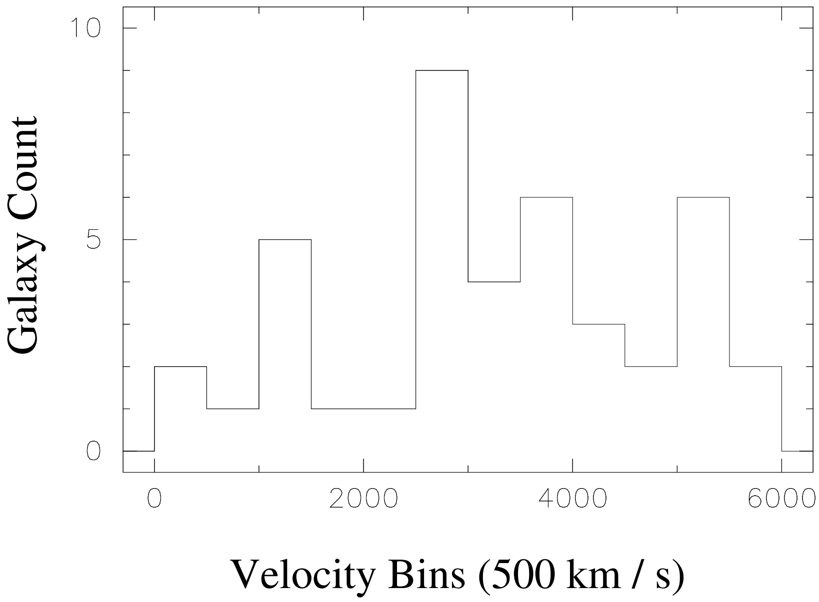

Fig. 5.— Velocity histogram of the H I detected galaxies in 500 km s^{-1} bins.

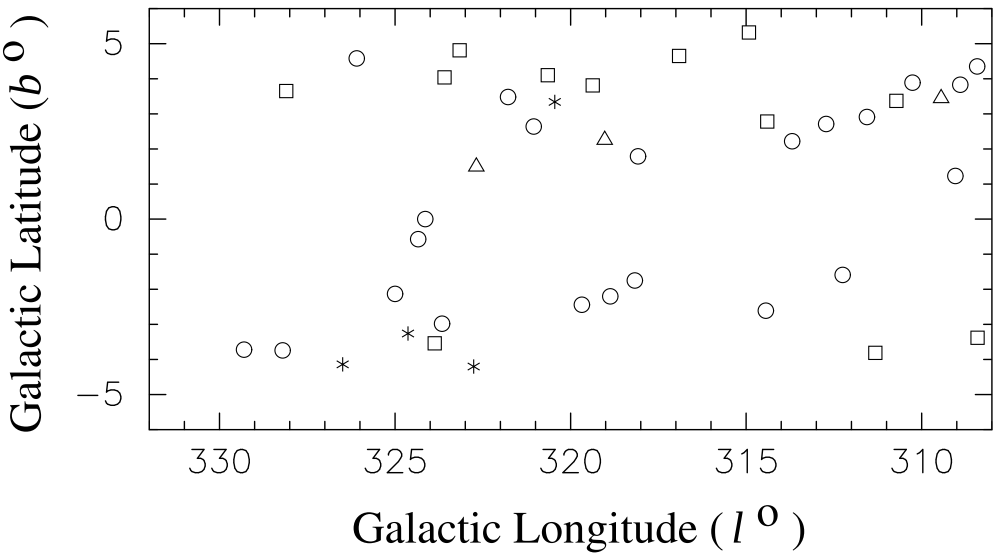

Fig. 6.— Distribution, in Galactic coordinates, of all H I detected galaxies. $\circ$: detections only found in H I, $\Box$: detections associated with optical and IRAS galaxies, $\triangle$: associated only with IRAS sources, $*$: detections with only optical associations.

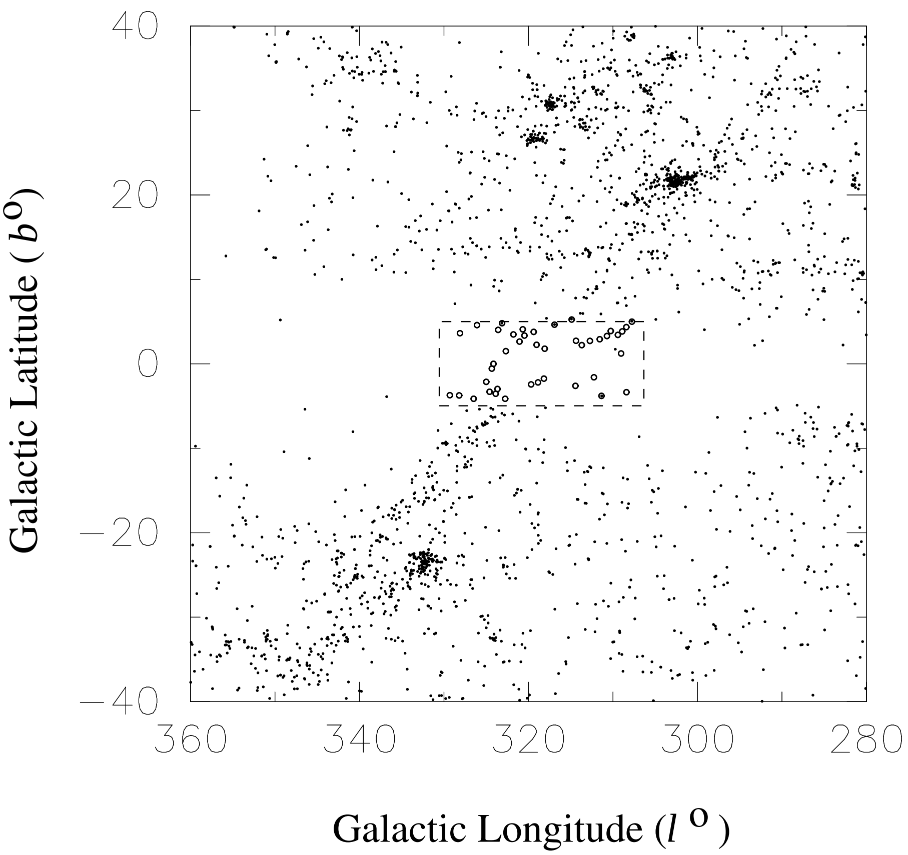

Fig. 7.— The distribution, in Galactic coordinates, of all optically identified galaxies with velocities within 6000 km s^{-1} (Lyon-Meudon Extragalactic Data Base) (dots). The new H I-detected galaxies (circles) are overlaid (previously known galaxies are filled circles). The dashed rectangle marks the extent of the region surveyed.

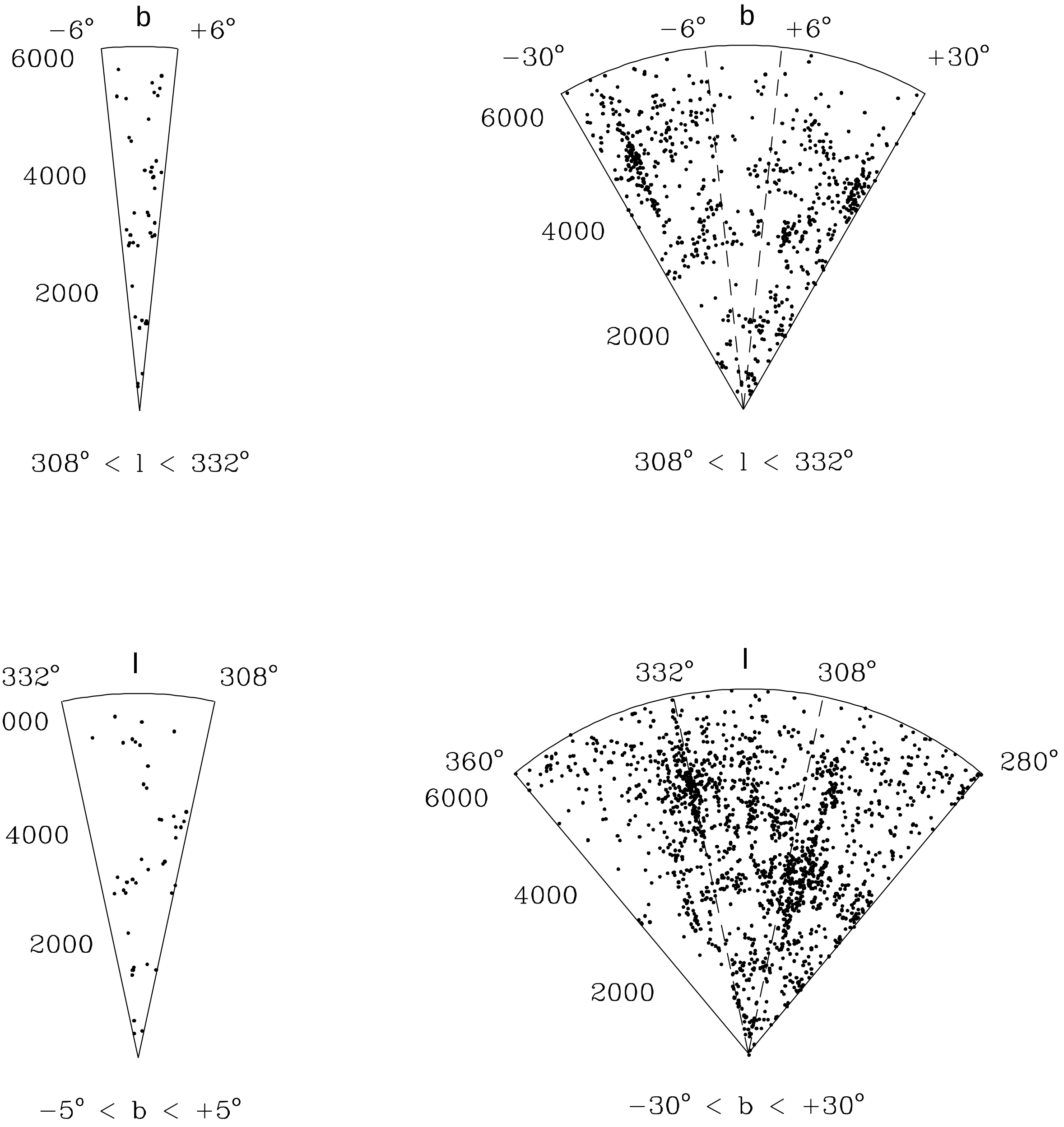

Fig. 8.— *Top left:* a cone diagram of the distribution in Galactic latitude and redshift (corrected to the Local Group frame) for the 42 galaxies detected. *Top right:* the latitude-redshift distribution including previously known galaxies (from LEDA) over a wider region, $-30^\circ < b < 30^\circ$. *Bottom left:* the Galactic longitude-redshift distribution for the new galaxies. *Bottom right:* the longitude-redshift distribution of previously known galaxies over a wider region $280^\circ < l < 360^\circ$. The Centaurus and Pavo clusters stand out as 'fingers of God' at $(l, b) = (302^\circ, 22^\circ)$ and $(332^\circ, -24^\circ)$, respectively.

Table 1. HI Data and Properties

Name	R.A. (J2000)	Dec. (J2000)	Gal. Long.	Gal. Lat.	Vel. Helio. (cz)	Vel. Width @50%	Dist. (LG)	Flux Integral	HI Mass
	h m s	d m s	deg.	deg.	km s^{-1}	km s^{-1}	Mpc	Jy km s^{-1}	$\times 10^9$ M$_\odot$
HIZOA J1327−57	13 27 26	−57 32 50	307.76	+4.99	2903	177	35.6	17.0	5.1
HIZOA J1333−58	13 33 00	−58 04 57	308.42	+4.35	1478	115	16.6	12.6	0.8
HIZOA J1337−58	13 37 16	−58 30 35	308.90	+3.83	4125	158	51.9	13.3	8.4
HIZOA J1341−58	13 41 48	−58 49 03	309.42	+3.42	3861	144	48.4	6.0	3.3
HIZOA J1342−61	13 42 12	−61 02 03	309.04	+1.23	3963	320	49.7	23.2	13.5
HIZOA J1344−65	13 44 52	−65 39 59	308.40	−3.36	2769	331	33.8	31.2	8.4
HIZOA J1347−58	13 47 19	−58 11 09	310.26	+3.89	3672	198	45.9	7.4	3.7
HIZOA J1351−58	13 51 40	−58 39 36	310.71	+3.30	3848	604	48.3	25.5	14.0
HIZOA J1358−58	13 58 43	−58 50 04	311.56	+2.91	4017	42	50.6	2.4	1.4
HIZOA J1407−58	14 07 47	−58 41 53	312.72	+2.71	3220	62	40.0	5.5	2.1
HIZOA J1413−65	14 13 26	−65 19 12	311.36	−3.80	449	246	3.0	1963.5	4.1
HIZOA J1414−62	14 14 46	−62 56 29	312.25	−1.59	3260	56	40.5	4.0	1.5
HIZOA J1416−58	14 16 03	−58 52 36	313.69	+2.22	5405	685	69.2	22.5	25.4
HIZOA J1417−55	14 17 10	−55 37 12	314.89	+5.25	3943	374	49.7	18.6	10.8
HIZOA J1419−58	14 19 40	−58 10 26	314.37	+2.73	3936	381	49.6	20.5	11.9
HIZOA J1432−55	14 32 03	−55 28 22	316.92	+4.64	3105	157	38.7	9.6	3.4
HIZOA J1436−63	14 36 02	−63 07 31	314.44	−2.61	1545	102	17.7	12.4	0.9
HIZOA J1448−57	14 48 12	−57 36 30	318.08	+1.79	4805	199	61.4	6.2	5.5
HIZOA J1450−55	14 50 17	−55 15 18	319.38	+3.78	5528	146	71.1	4.2	5.0
HIZOA J1452−56	14 52 59	−56 45 50	319.04	+2.26	3267	305	40.9	19.5	7.7
HIZOA J1457−54	14 57 15	−54 23 23	320.67	+4.09	2877	479	35.8	21.5	6.5
HIZOA J1458−55	14 58 32	−55 08 08	320.48	+3.35	5200	166	66.8	7.2	7.6
HIZOA J1501−60	15 01 22	−60 42 52	318.17	−1.75	4444	117	56.6	13.3	10.0
HIZOA J1504−55	15 04 25	−55 28 52	321.05	+2.64	5248	50	67.5	4.6	4.9
HIZOA J1505−54	15 05 59	−54 23 40	321.78	+3.48	2937	130	36.7	9.6	3.0
HIZOA J1508−60	15 08 10	−60 45 50	318.87	−2.20	4505	274	57.4	19.2	14.9
HIZOA J1509−52	15 09 16	−52 34 29	323.12	+4.81	1445	348	16.9	30.3	2.0
HIZOA J1514−52[a]	15 14 37	−53 00 53	323.59	+4.02	1445	428	16.9	152.6	10.3
HIZOA J1514−60	15 14 50	−60 33 33	319.68	−2.44	5146	363	66.0	12.0	12.3
HIZOA J1518−55	15 18 24	−55 37 50	322.68	+1.50	1491	235	17.5	12.4	0.9
HIZOA J1526−51	15 26 20	−51 11 16	326.09	+4.58	615	21	6.0	4.7	0.04
HIZOA J1532−56[a]	15 33 03	−56 04 07	324.14	+0.00	1365	55	15.9	28.2	1.7
HIZOA J1536−56	15 36 35	−56 25 20	324.34	−0.57	2722	176	34.0	11.7	3.2
HIZOA J1540−50	15 40 17	−50 48 42	328.11	+3.62	5323	77	68.9	6.2	7.0
HIZOA J1543−60	15 43 11	−60 13 37	322.76	−4.14	5193	241	66.8	13.4	14.1
HIZOA J1543−58	15 43 14	−58 45 28	323.66	−2.98	2897	143	36.3	11.3	3.5
HIZOA J1547−59	15 47 14	−59 04 23	323.87	−3.55	5631	310	72.7	10.3	12.8
HIZOA J1547−57	15 47 18	−57 16 05	325.00	−2.13	2769	89	34.6	6.5	1.8
HIZOA J1550−58	15 50 28	−58 26 18	324.60	−3.31	2059	109	25.1	5.5	0.8
HIZOA J1605−57	16 05 24	−57 51 12	326.48	−4.14	2991	89	37.7	15.1	5.0
HIZOA J1612−56	16 12 44	−56 23 48	328.20	−3.74	2729	291	34.3	11.2	3.1
HIZOA J1616−55[a]	16 18 16	−55 36 49	329.30	−3.72	403	101	3.3	31.4	0.08

[a]These galaxies have names derived from the more accurate ATCA positions (Staveley-Smith et al. 1998).

Table 2. H I derived Properties

Name	H I Diameter	Indicative Total Mass	M_{HI}/M_{total}	Morphology Estimate	Identification
	kpc	$\times 10^{10}$ $M_{\odot}$	%		
HIZOA J1413−65	32	7.4	5.6	Sc,Sd	Circinus
HIZOA J1436−63[a]	95	>5.7	<1.6	Sa	
HIZOA J1532−56[a]	108	>1.9	<8.9	Sc,Sd	
HIZOA J1616−55[a]	44	>2.6	<0.4	LSB	

[a] $i = 90^{\circ}$ assumed.

Table 3. Optical Data

Name	Optical Association	Offset	Velocity	Inclination	Source Morphology	Extinction	B_J (B-band)
	$< 6'$	arcmin	km s^{-1}	deg.		mag	mag
HIZOA J1327−57	ESO 173−G015	3.5	3006	82	S	16.3	3.5
HIZOA J1333−58							3.4
HIZOA J1337−58							3.9
HIZOA J1341−58							3.8
HIZOA J1342−61							10.5
HIZOA J1344−65	WKK 2503	1.3		63	S	15.2	3.8
HIZOA J1347−58							4.7
HIZOA J1351−58	WKK 2596	4.3	3867[a]	72	S	17.8	4.4
HIZOA J1358−58							3.2
HIZOA J1407−58							9.1
HIZOA J1413−65	Circinus	4.3	436	74	S	11.5	6.1
HIZOA J1414−62							13.1
HIZOA J1416−58							8.6
HIZOA J1417−55	WKK 3103	4.6	3954	82	S	15.0	2.7
HIZOA J1419−58	WKK 3132	4.1		75	S	19.6	6.6
HIZOA J1432−55	ESO 175−G009	1.1	3019	19	SB	14.6	3.6
HIZOA J1436−63							4.6
HIZOA J1448−57							7.3
HIZOA J1450−55	WKK 4352	2.8		42	S	17.6	4.0
HIZOA J1452−56							6.9
HIZOA J1457−54	WKK 4470	1.3	2877[a]	80	S	15.6	3.7
HIZOA J1458−55	WKK 4491	2.6		70	S	18.2	3.8
HIZOA J1501−60							8.3
HIZOA J1504−55							6.2
HIZOA J1505−54							4.3
HIZOA J1508−60							5.6
HIZOA J1509−52	ESO 223−G012	3.5	1283	88	S	14.1	3.3
HIZOA J1514−52	WKK 4748	1.7	1451[a]	80	S	13.9	4.3
HIZOA J1514−60							6.1
HIZOA J1518−55							14.2
HIZOA J1526−51							2.7
HIZOA J1532−56							69.1
HIZOA J1536−56							33.3
HIZOA J1540−50	WKK 5182	2.7		34	E	17.4	3.6
HIZOA J1543−60	WKK 5229	4.9		75	S	15.8	3.1
HIZOA J1543−58							4.9
HIZOA J1547−59	WKK 5285	0.8		54	S	17.1	2.8
HIZOA J1547−57							6.0
HIZOA J1550−58	WKK 5366	3.9		74	S	16.4	3.1
HIZOA J1605−57	WKK 5834	1.4		60	S	17.0	2.1
HIZOA J1612−56							2.3
HIZOA J1616−55							2.8

[a] Velocities from Woudt & Kraan-Korteweg (2000), may not be final.

Table 4. IRAS Data

Name	IRAS Association	Offset		IRAS flux densities[a]		
			12μm	25μm	60μm	100μm
	$< 6'$	arcmin	Jy	Jy	Jy	Jy
HIZOA J1327−57	IRAS 13242−5713	4.0	1.21B	7.52B	76.32C	89.86D
HIZOA J1341−58	IRAS 13386−5832	2.8	0.37C	0.86C	3.95D	4.04G
HIZOA J1344−65	IRAS 13413−6525	1.1	0.38L	1.07C	7.81C	13.47C
HIZOA J1351−58	IRAS 13483−5820	4.8	0.25L	0.25L	1.22D	19.26G
HIZOA J1413−65	IRAS 14092−6506	5.5	18.80B	68.44B	248.70C	315.90C
HIZOA J1417−55	IRAS 14137−5518	5.3	0.28L	0.25E	2.56C	7.10C
HIZOA J1419−58	IRAS 14159−5755	3.3	0.45L	0.25L	1.59C	2.84G
HIZOA J1432−55	IRAS 14284−5514	1.9	0.34C	0.53D	6.06C	13.23C
HIZOA J1450−55	IRAS 14464−5501	4.2	0.41L	0.25L	0.94C	2.75G
HIZOA J1452−56	IRAS 14492−5634	1.1	0.27L	0.45C	3.89C	4.05G
HIZOA J1457−54	IRAS 14535−5411	1.7	0.40L	0.25L	1.60B	6.69E
HIZOA J1509−52	IRAS 15058−5221	3.0	0.38L	0.33B	4.44B	17.80C
HIZOA J1514−52	IRAS 15109−5248	1.6	0.79C	0.99B	18.23C	60.23C
HIZOA J1518−55	IRAS 15147−5527	1.4	1.73L	1.07L	2.19D	6.31G
HIZOA J1540−50	IRAS 15364−5038	3.3	0.51L	0.45C	3.31C	5.22G
HIZOA J1547−59	IRAS 15431−5855	0.5	0.43L	0.32F	2.11E	10.02D

[a]The following key explains the uncertainties in the IRAS fluxes (IRAS Explanatory Supplement, Beichman et al. 1985). B: 4% $\leq$ uncertainty $<$ 8%, C: 8% $\leq$ uncertainty $<$ 12%, D: 12% $\leq$ uncertainty $<$ 16%, E: 16% $\leq$ uncertainty $<$ 20%, F: uncertainty $\geq$ 20%, L: Upper Flux Limit, and G: IGA Source Flux Estimate $\pm$30% (the IGA was used when the IRAS PSC gave only upper limits at 60 and 100μm).